**Научном већу Института за физику**
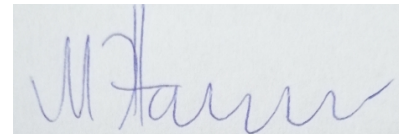
Београд 12.10.2021.


**Предмет: Покретање поступка у звање истраживач сарадник**

Молим научно веће Института за физику у Београду да покрене поступак за мој избор у звање **Истраживач сарадник**, имајући у виду да испуњавам све критеријуме прописане од стране Министарства просвете, науке и технолошког развоја Републике Србије за стицање наведеног звања.


У прилогу достављам:

1. Мишљење руководиоца лабораторије са предлогом комисије за избор у звање;
2. Стручну биографију;
3. Преглед научне активности;
4. Списак и копије објављених научних радова и других публикација;
5. Уверење о последњем овереном и уписаном семестру на докторским студијама;
6. Фотокопија диплома са основних и мастер студија;
7. Потврда о прихватању теме докторске дисертације;


С' поштовањем,

_____

Медић Жарко
истраживач приправник

Београд 12.10.2021.

**Научном већу Института за физику**

**Предмет: Мишљење руководиоца лабораторије за избор Медић Жарка у звање истраживач сарадник**

Медић Жарко завршио је основне, а потом и мастер академске студије на Природно-математичком факултету Универзитета у Новом Саду. Докторске студије из физике уписао је 2015. године. Положио је све испите предвиђене планом. Тема његове докторске дисертације представљена је и прихваћена од стране Научно-наставног већа Природно-математичког факултета Универзитета у Новом Саду. Ангажован је у Лабораторији за 2Д материјале и бави се проблемима изучавања 2Д материјала и њихове интеракције са зрачењем.

С обзиром да Медић Жарко испуњава све услове предвиђене Правилником о поступку и начину вредновања и квантитативном исказивању научноистраживачких резултата истраживача, сагласна сам са покретањем поступка за избор у звање истраживач сарадник.

За чланове комисије за избор Медић Жарка у звање истраживач сарадник предлажем следећи састав:


1. др Борислав Васић, виши научни сарадник, Институт за физику Београд
2. др Радош Гајић, научни саветник у пензији, Институт за физику Београд
3. проф. др Миодраг Крмар, редовни професор, Природно-математички факултет у Новом Саду


Руководилац лабораторије за 2Д материјале

Ивана Милошевић
научни сарадник

# Стручна биографија Медић Жарка

Медић Жарко је рођен 1988. године у Новом Саду. Након завршене основне школе и гимназије "Јован Јовановић Змај" уписује основне академске студије из физике 2007. године на Природно-математичком факултету у Новом Саду. Студије завршава 2013. године одбраном дипломског рада под називом "Koliko su Ge(n, ϒ) reakcije merodavne za procenu fluksa termalnih neutrona".

Мастер академске студије физике уписује 2013. године, усмерење нуклеарна физика, на Природно-математичком факултету у Новом Саду. Студије завршава 2014. године одбраном мастер тезе под називом "Simulacija svojstava neutronskog reflektometra". Мастер рад је настао током студијских боравака у Helmholtz Zentrum у Немачкој.

Докторске академске студије физике уписује на Природно-математичком факултету 2015. године. Током 2018. године запошњава се као истраживач приправник на Институту за физику Београд у лабораторији за графен, друге 2Д материјале и уређене наноструктуре.

Током периода рада на Институт за физику под менторством др Радоша Гајића, изучава технике раста монокристала са нагласком на Брицманом метод и лебдећу зону. Бави се ексфолијацијом материјала посредством микромеханичке, течне и термалне методе. Од тако ексфолираних флека покушава депоновати исте на супстрат ради добијања танких филмова. Упоредо са тим изучава понашања танких филмова и монокристала у пољу алфа, електрона, х и гама зрака. Изучава атомске процесе и процеси на нивоу језгра.

До сада је аутор 4 научна рада у међународним часописима.

# Преглед научне активности

Током своје научне каријере Медић Жарко се бавио изучавањем синтезе материјала и интеракције зрачења са материјалима. Какве ефекте зрачење постижу на нивоу језгра и атомском нивоу. Циљ његовог истраживачког рада је разумевање принципа по којим се зрачење простире кроз материјале и начине на које оно интерагује са материјом.

Интеракција гама зрачења са језгром индијума-115

Потреба за тачним одређивањем ефикасног пресека за интеракцију зрачења са атомским језгрима је од суштинског значаја за могућност тачних прорачуна нуклеарних процеса у којима су укључена атомска језгра. Коришћени су танки дискови од природног индијума који у свом саставу има два стабилна изотопа (индијум-113 и индијум-115). Такви дискови су потом озрачавани у пољу закочног зрачења, ово је све рађено по NAXSUN методи. Посредством овога метода је могуће извршити меру присуства гама фотона и неутрона у одређеној области. Озрачавање вршено је микротроном, а детекција гама спектроскопском апаратуром. Обрада резултата вршена је посредством unfolding алгоритма MAXED и GRAVEL. У раду коришћен је и Монте Карло метод ради добијања интензитета и облика спектралне функције закочног зрачења.

Синтеза титанијум диоксида посредством метода лебдеће зоне

Метода лебдеће зоне омогућава добијење кристала са веома ниским садржајем дефеката. Тако добијени жути кристал са минималним садржајем дефеката и плави кристал са мало већим садржајем дефеката. Узорак је карактеризован са Раман , EDS и XRD методом.

Интеракција алфа, бета и гама зрака са монокристалним узорком титанијум диоксида

По доступној литератури оптичка влакна од титанијум диоксида су коришћени за пренос светлосног сигнала. Из тога разлога су вршена истраживања могућих промена у нивоу дефеката и структури  услед озрачавања са зрачењем. Узорак пре и после озрачавања је карактеризован са Раман , EDS и XRD методом. Од зрачења коришћено је алфа, бета и гама зрачење, тако да је по један узорак (жути и плави) озрачен са једним типом зрачења.

Синтеза графена

Овде је циљ научити методе синтезе 2Д графенског филма. Поступак синтезе је у прво време вршен микромеханичком ексфолијацијом, при цему је нагласак био на прављењу што тањих флека ради изучавања интеракције графена и супстрата SiO2/Si.

Након тога рађена је течна ексфолијација којом је било могуће добити довољно диспергованог материјала за добијање танких филмова са Langmuir-Blodgett методом.

Интеракција гама и x зрака са графеном

Показано је да графен поседује високе електрично и термичко проводне карактеристике због чега је његова примена у електроници интересантна. Из тога разлога извршено је озрачавање танких графенских филмова добијених Langmuir-Blodgett методом. Направљен је сет плочица које су озрачене са x зрацима. Графенски узорци су пре и после озрачавања карактерисани са Раман и XRD методом. Вршена су и транспортна мерења пре и после озрачавања. Гама фотонима озрачене су пар узорака. Једно мерење је вршено током самог процеса озрачавања.

Синтеза пирофилита

Циљ рада је био развити поступак за прављење таниких пирофилитних филмова. Поступак је отпочео са микромеханичком ексфолијацијом ради изучавања интеракције танког филма са субстратом SiO2/Si.

Потом се течном ексфолијацијом добио одређени степен диспергованих флека у раствору. Истраживања везана за овај тип ексфолијације су још у току ради прављења максимално оптимизоване руте којим би се материјал могао ексфолирати. У ужем смислу танки филм од овог материјала још није направљен са Langmuir-Blodgett методом.

Познато је да се пирофилит може на повишеним температурама ексфолирати поступком разлиставања. Полазећи од те особине тренутно је истраживање у правцу проналажења оптималних услова за термалну ексфолијацију како кристала тако и танких пирофилитних флека које су добијене посредством микромеханичке ексфолијације. На овај начин ексфолирани материјал би могао да попуни простор око полазног материјала и на тај начин изгради танак

филм. Ова метода се исто налази у фази развијања. Први резултати указују да овај смер има потенцијал.

Карактеризација дебљине материјала рађена је посредством AFM уређаја, а промене у структури и ниво дефектности исте посредством Раман и XRD методе. Степен диспергованих пирофилитних флека у раствору мерен је са UV/VIS методом.

**Списак и копије објављених научних радова и других публикација**

1. Medic, Z., Jovancevic, N., Maletic, D. *et al.* The application of the unfolding technique for determination of photo-nuclear reaction cross-section with an example on the 115In(γ,γ′)115mIn reaction. *Eur. Phys. J. A* 57, 258 (2021). https://doi.org/10.1140/epja/s10050-021-00567-9

Regular Article - Experimental Physics

# The application of the unfolding technique for determination of photo-nuclear reaction cross-section with an example on the $^{115}$In$(\gamma,\gamma')^{115m}$In reaction

Z. Medic[1], N. Jovancevic[1,a], D. Maletic[2], Y. Teterev[3], S. Mitrofanov[3], A. Belov[3], M. Krmar[1], M. Hult[4], S. Oberstedt[4]

[1] Physics Department, Faculty of Sciences, University of Novi Sad, Novi Sad, Serbia
[2] Institute of Physics, Belgrade, Serbia
[3] Flerov Laboratory of Nuclear Reactions, Joint Institute for Nuclear Research, Dubna, Russia
[4] European Commission, Joint Research Centre (JRC), Geel, Belgium

**Abstract** The cross-section function for the $^{115}$In$(\gamma,\gamma')^{115m}$ In reaction was determined in the energy range up to $E_\gamma$ = 9.6 MeV using the bremsstrahlung facility at the MT25 Microtron, JINR, Dubna. Natural indium disks were irradiated with bremsstrahlung, each disk with a beam of different endpoint energy. To the measured saturation activity built up in the wide-energy photon beam we applied the unfolding technique, developed recently at the JRC-Geel with the primary purpose of being used in neutron activation. The results were compared with TALYS 1.9 calculations and existing experimental data. Our results suggest that the application of existing unfolding technique allow determining unknown excitation functions of photon-induced reactions.

## 1 Introduction

Experimental data obtained in nuclear reactions induced by photons on various materials are important for a number of different applications. High-energy photons are used to produce radionuclides for medicine and other applications. They are used in radiotherapy, industry, activation analysis and play significant roles in astrophysical processes and in the dynamics of nuclear reactors [1]. Therefore, cross-sections of photo-nuclear reactions are often studied in a wide energy region. The rich amount of experimental results obtained, can be found in several databases such as Refs. [2–8].

The aim of this paper is to apply the NAXSUN technique (Neutron Activation X-Section determined using UNfolding) to determine the differential cross section for the excitation of the 336.2 keV isomer in $^{115}$In as a function of the photon

energy, using photons from bremsstrahlung beams of several different endpoint energies. The NAXSUN technique was developed at the JRC-GEEL and utilized to obtain neutron-induced reaction cross sections as a function of incident neutron energy [9–13]. For the photo-activation measurements we adapted the NAXSUN technique and examined its applicability in photon-induced reactions.

There are several reasons why the excitation of $^{115}$In isomer state was chosen to test the possibility of extending the NAXSUN technique to the field of photo-nuclear reactions. Natural indium is a mixture of two isotopes $^{113}$In (4.3%) and $^{115}$In (95.7 %) [14]. It is a soft metal that is easy to shape in the desired irradiation and detection geometry. It can be used in several different ways as an activation detector for neutrons or photons. The high thermal neutron cross section of 160 b [15] has made $^{115}$In a frequently used nuclide for neutron monitoring. The excitation of the 336.2 keV [14] isomeric state by non-elastic neutron scattering, $^{115}$In$(n,n')^{115m}$In, is recognized as one of the most common reactions for detection and monitoring of fast neutrons. Moreover, detection of photons having energies higher than 9 MeV (produced by LINAC-s used in radiotherapy, for example), which is the threshold energy for the photo-nuclear reaction $^{115}$In$(\gamma,n)^{114}$In, is possible by using activation foils made of natural indium. And finally, high-energy photons may excite the isomeric state via the reaction $^{115}$In$(\gamma,\gamma')^{115m}$In.

All these reactions make indium the material of choice in experimental circumstances, when it is necessary to register the presence of neutrons and photons at the same location. For neutron reactions on $^{115}$In cross sections are well known, and reliable data on the differential cross section for the $^{115}$In$(\gamma,n)^{114}$In reaction are available, too. There are several experimental data sets [16–20], included in database [8],

for photo-excitation of the $^{115m}$In isomeric state. The cross-section values of the $^{115}$In$(\gamma,\gamma')^{115m}$In reaction and the shape of the cross-section function in those several sources differ somewhat (datasets are shown in Fig. 12). Furthermore, data available in literature [8], show discrepancy with TALYS 1.9 [21,22] calculations, as can be seen in Figs. 11 and 12, below in this text. Additional objective of this paper is to report on a new measurement of the $^{115}$In$(\gamma,\gamma')^{115m}$In cross section.

Possible applicability of NAXSUN techniques in photnuclear reactions can open a broad research field. Differential cross sections for $(\gamma,$n$)$ reactions are well documented with reliable experimental material. However, at higher photon energies, when two or more neutrons are emitted, the results of measuring the flux-weighted averaged cross section and measurements with quasi-monoenergetic photon beam can be found in the literature [2,3,8]. For a specific channel of $(\gamma,$xn$)$ nuclear reactions, energy differential cross-sections can be obtained using theoretical calculations only. The introduction of the NAXSUN techniques could make it possible to measure energy differential cross-sections for these nuclear reactions as well.

## 2 The method

The NAXSUN technique is based on irradiation of several identical metal disks in different, but overlapping, neutron fields. It is followed by gamma-spectrometric measurements and unfolding procedures. This method has solely been used for measuring cross section curves for neutron-induced reactions [11–13].

The yield of activation products from some nuclear reactions, here the photo-excitation of the first excited and metastable state in $^{115}$In in a bremsstrahlung beam, can be quantified by its saturation activity (maximum equilibrium activity when the rate of production of reaction product equals the rate of decay) $A$:

$$A = \int_{E_{th}}^{E_{max}} \sigma\,(E) \cdot \Phi\,(E) \cdot dE \qquad (1)$$

where $\sigma\,(E)$ is the cross section for the studied nuclear reaction, $\Phi(E)$ is the flux spectrum of incident photons and E is the photon energy. $E_{th}$ is the energy threshold for the nuclear reaction and, $E_{max}$ is the endpoint energy of the bremsstrahlung beam. After exposure to the photon beam, the induced activity of $^{115m}$In is measured by a high energy resolving $\gamma$-spectrometer.

One indium disk at the time was exposed in a bremsstrahlung beam of particular endpoint energy. The endpoint energies ranged from 5 to 10 MeV. In this way disks were exposed to different but overlapping photon fields, similar to the measurements performed in our previous work, where broad-energy neutrons fields were applied [11–13]. After irradiation

the saturation activity of each of the six disks is determined by $\gamma$-spectromety.

If the photon flux-spectrum, $\Phi(E)$ can be estimated, as shown in Section III D. in this paper, the general task comes down to the solution of six integral equations (Eq. 1) for each irradiated sample, and the determination of the unknown function $\sigma$(E), which describes the cross section of the photonuclear reaction. Having six known values of saturation activity, $A$, the problem can be transformed into a system of discretized equations:

$$A_k = \sum_i^c \Phi_{ik} \cdot \sigma_i \cdot \Delta E_i; \quad k = 1, 2, ...m \qquad (2)$$

where $A_k$ is the measured saturation activity of each irradiated disk, $k$, with $m$ activated disks, $k$ running from 1 to 6. The photon flux for a certain energy bin, $E_i$ and disk $k$ is described by $\Phi_{ik}$. $\Delta E_i$ is the width of energy bin $i$, and $c$ is the number of energy bins. $\sigma_i$ represents the sought cross section function. Since $c$ is larger than $m$ the system of equations is under-determined and an unfolding procedure needs to be applied. In this work, we used three unfolding algorithms, SANDII, GRAVEL and MAXED [23–27], to take into account corresponding systematic uncertainties.

## 3 Measurements

### 3.1 Material

Six identical metal disks of indium with natural isotopic abundances were used. The material has a high level of purity with 99.9% of natural indium. Disks had an identical shape with a diameter of 20.0(1) mm and and an average thickness of 0.210(1) g cm$^{-1}$. Two more indium discs were used to check influence of neutrons on excitation of $^{115}$In isomer state. Sources of neutrons are described in next section.

### 3.2 Irradiation

All experimental activities were performed at the Flerov Laboratory of Nuclear Reactions of the JINR, Dubna. The MT25 Microtron [28] was used to produce the bremsstrahlung beams for irradiation of the indium disks. A more detailed description of the Microtron and the experimental setup can be found in Ref. [29]. Indium disks were exposed to bremsstrahlung with endpoint energies from 5 to 10 MeV in steps of 1 MeV (Table 1). For the photon production we used a 1 mm thick tungsten radiator. The distance between the the radiator and an indium disk was 60 cm.

An 8 mm thick beryllium plate was placed in front of the In sample, 52.5 cm far from the tungsten radiator, to serve in another study [29]. The influence of the beryllium plate on
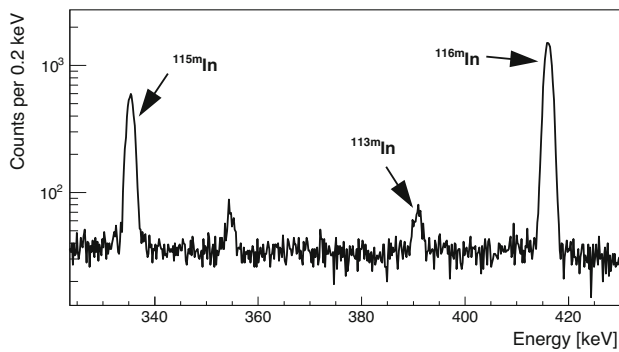
**Fig. 1** Part of the $\gamma$-ray spectrum collected after irradiation of indium disk No. 6. The $\gamma$ lines of interested are labelled. Energy width of one channel is 0.2 keV

the photon flux was corrected by Monte Carlo simulation as described below. The scheme of the experimental set up is presented in the Fig. 2.

Energy thresholds for photo-disintegration of $^9$Be (followed by emission of neutron) and $^{183}$W($\gamma$,n)$^{182}$W are 1.7 MeV and 6.2 MeV respectively [30]. In order to minimize the influence of inelastic neutron scattering, $^{115}$In(n,n')$^{115m}$In reaction, the indium disks were placed in the center of a water container with a diameter of 15 cm. In this way, fast neutrons created in photo-nuclear reactions in beryllium and tungsten are thermalized. The need for such an action was confirmed by a noticeable difference in $^{115m}$In activity, after exposure with and without water around the indium disk. At a maximum photon energy of 23 MeV the saturation activity of $^{115m}$In in the disk exposed outside the water container was 15% higher than the saturation activity of $^{115m}$In, when the disk was located inside the water container. Furthermore, we may expect significantly lower parasitic neutron production at lower energies. We observed too that the saturation activity of $^{116}$In produced by neutron capture is about 130 times lower at a photon-energy of 10 MeV than at endpoint energy of 23 MeV. This means that there is an insignificant influence of non-elastic scattering of high-energy neutrons on the excitation of the isomeric state in $^{115}$In with samples placed in the water container.

The irradiation time was longer for lower photon-energies and ranged from 14 min at 10 MeV to 98 min at 5 MeV. The Microtron electron current varied from 2 to 7 $\mu$A. The integral number of electrons striking the tungsten radiator ($Q$) is summarized in the Table 1.

### 3.3 Gamma spectroscopy measurements

After exposure, the decay spectra of the indium disks were measured using an HPGe detector. The relative efficiency of the detector was 25% and, it was passively shielded by 5 cm of lead. The irradiated indium disks were located directly on

the vertical end-cap of the detector. The elapsed time between the end of the irradiation and the start of each measurement was between 6 min and 2 h depending on detector availability. Considering that the half life of $^{115m}$In is $T_{1/2} = 4.468$ h [14], in the worst case, more than 73% of initial activity remained. The measurement time for each activated disk was 30 min that was sufficient to obtain good counting statistics. For example, in the spectrum of that indium disk exposed to the 7 MeV bremsstrahlung beam the statistical uncertainty of the $^{115m}$In gamma line was about 3% at 1 $\sigma$.

The recorded spectra have very simple structure (part of the $\gamma$-ray spectrum collected after irradiation of indium disk No. 6. is presented in Fig. 1). In all of them the prominent 336.2 keV gamma line from the de-excitation of the isomeric level in $^{115m}$In is observed. The gamma line of the isomeric state of $^{113m}$In, $E_\gamma = 391.7$ keV [14], is noticeable in some of measured spectra, especially in the spectrum from the indium disk exposed at 10 MeV endpoint energy as depicted in Fig. 1. In the $\gamma$-ray spectrum of the disk exposed to the 5 MeV bremsstrahlung, the 391.7 keV gamma line is not observed at all. The reason is the low abundance of $^{113}$In in natural indium, i.e. 4.3 % in combination with the small flux at 5 MeV. Several other gamma lines (416.9 keV, 1097.3 keV and 1293.5 keV [14]) emitted after the decay of $^{116m}$In, produced by neutron capture of $^{115}$In, appeared only in spectra of those indium disks exposed at higher endpoint energies.

The saturation activity of $^{115m}$In can be determined from the peak area of the 336.2 keV gamma line according to:

$$A_k = \frac{N_\gamma \cdot M\lambda}{m \cdot N_A \cdot \epsilon \cdot \eta \cdot p_\gamma \cdot e^{-\lambda \Delta t} \cdot \left(1 - e^{-\lambda t_{irr}}\right) \cdot \left(1 - e^{-\lambda t_m}\right)}$$

(3)

where $N_\gamma$ is the number of detected $\gamma$ rays with $E_\gamma = 336.2$ keV, $\lambda$ is the decay constant, $M$ and $m$ are the mass number and the mass of the In disk used, $N_A$ is Avogadro constant , $\epsilon$ is the total efficiency of the detector at 336.2 keV, $\eta$ is the natural abundance of $^{115}$In, $p_\gamma$ is a gamma emission probability, $\Delta t, t_{irr}$ and $t_m$ are cooling, irradiation and measurement time, respectively. Total efficiency was determined using calibration sources and LabSOCS software. Since indium is a soft metal, our samples were designed to match existing detector calibrations.

We notice that the saturation activity for $E_{max} = 5$ MeV is almost 150 times lower than the one at $E_{max} = 10$ MeV. All saturation activities, $A_k$, are summarized in Table 3. The statistical uncertainty at 5 MeV and at 6 MeV is about 10 % and, above 7 MeV the statistical uncertainty is up to 4 %.

**Table 1** Irradiation characteristics for each indium disk: $E_{max}$ bremsstrahlung endpoint energy, $Q$ integral number of electrons striking tungsten target, $t_{irr}$ time of irradiation

| Disk no. | $E_{max}$ (MeV) | $Q$ (mAs) | $t_{irr}$ (s) |
|---|---|---|---|
| 1 | 5.00(5) | 12 | 5880.0(5) |
| 2 | 6.00(5) | 10 | 1320.0(5) |
| 3 | 7.00(5) | 12 | 1740.0(5) |
| 4 | 8.20(5) | 3.5 | 1680.0(5) |
| 5 | 9.00(5) | 7 | 1020.0(5) |
| 6 | 10.00(5) | 6 | 840.0(5) |

## 3.4 Determination of photon flux

### 3.4.1 Monte Carlo simulation

The application of unfolding procedures to our problem requires information about the $\Phi_{ik}$ from Eq. 1, i.e. shape and intensity of the bremsstrahlung photon spectra. This was obtained using Monte Carlo (MC) simulations and the measured values of the integral number of electrons striking the tungsten radiator.

To estimate the flux of incident photons $\Phi(E)$ for the six used energies we employed Geant4 (G4) version 10.05.p01 [31] with the experimental Physics list QBBC. QBBC uses the standard G4 electromagnetic physics option without optical photon simulations and, the hadronic part of this physics list consists of elastic, inelastic, and capture processes. Each hadronic process is built from a set of cross sections and interaction models, which provide the detailed physics implementation.

Figure 2 depicts the setup geometry as entered to the Geant4 simulations. Elements of simulations are starting from the electron beam, shown to the left of the figure, going to the indium disk placed in the water container on the right. In the G4 simulations electron beam starting position is 10 cm before Cu foil.

The geometry of the Geant4 simulations consists of an electron beam of six energies, assuming a $\pm 1\%$ uncertainty (k = 1) for all energies. Then, on the beam path comes first a 70 μm thick copper foil followed by a copper cylindrical collimator with a 12 mm-wide circular hole. Next comes a 1 mm thick tungsten radiator followed by a 2 cm thick aluminium block. The distance between the tungsten radiator and the indium disk is 60 cm. In front of the indium disk we placed an 8 mm thick beryllium sheet and the water shielding. We simulated about $2 \times 10^8$ electrons for six different electron beam energies. From the simulation we obtained the integral number of photons, spectrum shape and the distribution of photons on the surface of an indium disk for each energy. To get approximation of integral number of gammas, which hit the indium sample, the number of photons from the simulation were scaled, having in mind that the number
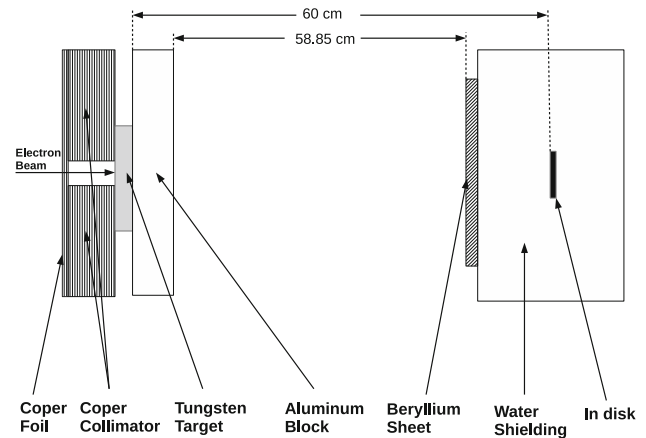


**Fig. 2** Geometry of experimental setup (not in scale)
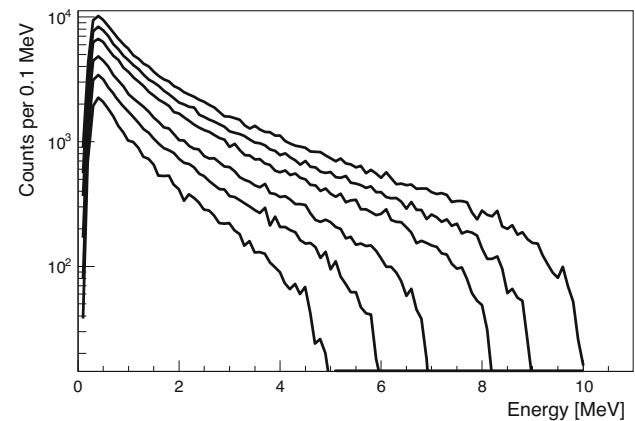


**Fig. 3** Spectra of photon flux on the indium disks for all electrons energies incident on the tungsten radiator. The electron energy corresponds to the end-point energy of the respective photon-flux spectrum ($E_{max}$ in the Table 1)

of electrons per mAs is $6.242 \times 10^{15}$ and that each beam energy had a different number of electrons per second. The estimated integral number of photons hitting an indium disk at the particular endpoint energy is shown in the last column of Table 2. The simulated photon spectra are depicted in Fig. 3.

**Fig. 4** The photon distribution on the surface of an indium disk, simulated for the endpoint energy 10 MeV
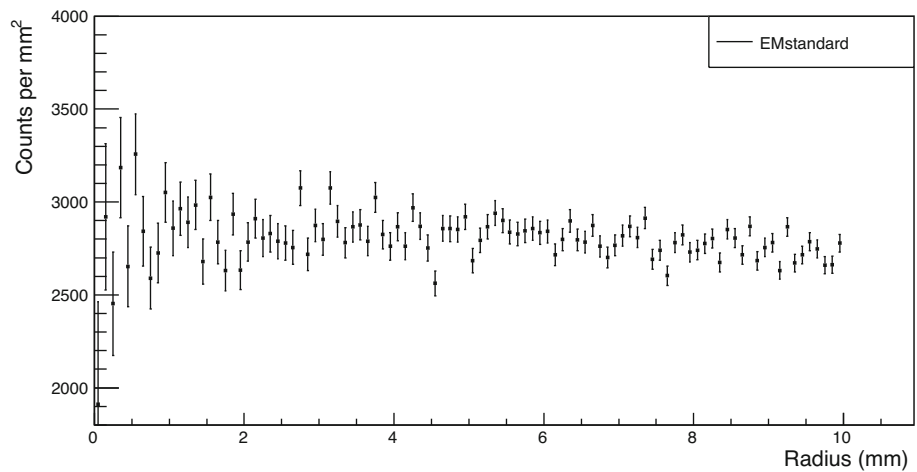


**Table 2** Irradiation characteristics of the indium disks: $E_{max}$ endpoint energy, $N_{e,S}$ simulated number of electrons, $N_{\gamma,S}$ simulated number of photons, $S$ scaling factor, $N_{\gamma Scaled}$ scaled number of photons

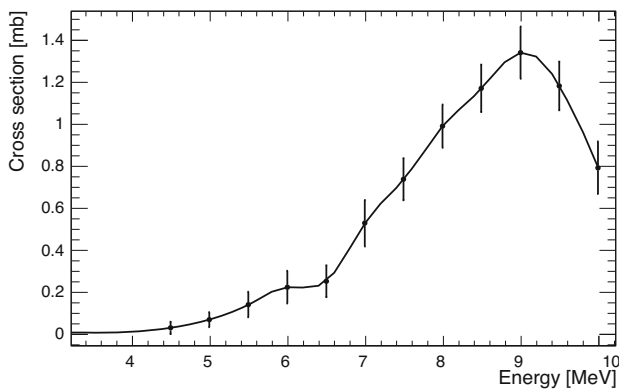| E (MeV) | $N_{e,S}$ ($10^6$) | $N_{\gamma,S}$ | $S$ ($10^7$) | $N_{\gamma Scaled}$ ($10^{12}$) |
|---|---|---|---|---|
| 5.00(5) | 200 | 25312 | 3.12 | 9.48 |
| 6.00(5) | 199 | 43163 | 3.14 | 13.54 |
| 7.00(5) | 194 | 65120 | 3.22 | 25.14 |
| 8.20(5) | 192 | 99595 | 3.25 | 11.33 |
| 9.00(5) | 192 | 129258 | 3.25 | 29.42 |
| 10.00(5) | 187 | 165313 | 3.34 | 33.11 |



**Fig. 5** Cross section for $^{113}In(\gamma, \gamma')^{113m}In$ reaction (points – measured data [32], line – spline interpolation)

In Fig. 4 the simulated areal distribution of the photon flux on the indium disks is shown for the 10 MeV endpoint energy. The distribution is flat across the entire disk. Corresponding results were obtained for the other endpoint energies.

### 3.4.2 Normalization of photon flux

To obtain absolute cross section values, it is necessary to have accurate values of the photon flux at the place of the exposed indium disks. In our experimental setup, the total number of electrons striking the tungsten radiator, expressed in mAs in Table 1, could only serve as a relative measure. For the absolute calibration of the Monte-Carlo simulated photon spectra, it was necessary to use another nuclide with well-known photo-activation cross section. In the absence of some well-accepted standard, it was decided to use the photo-activation of $^{113}$In for spectrum normalisation. As can be seen in Fig. 1, the characteristic gamma line of $^{113m}$In is present in the spectrum after irradiation of the indium samples at higher energies. The cross section function for the reaction $^{113}In(\gamma, \gamma')^{113m}In$ was taken from Ref. [32] as depicted in Fig. 5. In this study, samples of natural indium were irradiated in the range of 4–12 MeV with 0.5 MeV increments. The cross section was calculated using Penfold-Leis method [33]. Photon flux was determined using an absolutely calibrated ionization chamber with a build-up cap of appropriate thickness.

Saturation activity for $^{113}In(\gamma, \gamma')^{113m}In$ reaction at some chosen energy, $A_c$, can be calculated based on the Eq. 2. Photon flux spectra were calculated using Monte-Carlo simulation with a number of incident electrons specified in Table 2. Simulated spectra were corrected by Microtron electron current $Q$, as a relative measure, taken from Tab. 1. Interpolated values of the cross-section from Fig. 5 were taken to calculate the saturation activity $A_c$ for the 10 MeV photon beam. The measured values of the saturation activities for the

**Table 3** Saturation activity, $A_k$, for a given endpoint energy, $E_{max}$ calculated according to Eq. 3

| Disk No. | Energy [MeV] | $A_k[10^{-18}$ Bq/atom] |
|---|---|---|
| 1 | 5.00(5) | 0.0090(9) |
| 2 | 6.00(5) | 0.044(5) |
| 3 | 7.00(5) | 0.161(7) |
| 4 | 8.20(5) | 0.191(5) |
| 5 | 9.00(5) | 0.87(3) |
| 6 | 10.00(5) | 1.33(3) |

$A_m$ obtained using the intensity of the 391.7 keV gamma line detected for 10 MeV was $1.10(18) \times 10^{-18}$ Bq/atom. Based on that, a normalization factor of $r = A_m/A_c = 6.2(11)$ was obtained and used to normalise photon spectra, which were used in unfolding procedures.

## 4 Experimental results

### 4.1 Default functions for unfolding procedures

Cross-section unfolding procedures require an initial guess of the sought function, the so-called default function, to proceed further with the unfolding calculation. This function should be a reasonably good guess of the real cross-section function. In this work we used the TALYS 1.9 code [22] for determining this default functions.

TALYS 1.9 is a computer code for the simulation of nuclear reactions. A detailed description of TALYS 1.9 can be found in Ref. [22]. By this code it is possible to calculate various physical quantities for all possible outgoing reaction channels using different physical models in the calculations. In this work we calculated the cross section for the $^{115}$In$(\gamma, \gamma')^{115m}$In reaction, for incident photon energies ranging from 0 to 10 MeV. All parameters of calculations were code-default values except level density parameters. Available level density models in the TALYS 1.9 are [34–42]:

- LD model 1. – the constant temperature Fermi-Gas model;
- LD model 2. – the back-shifted Fermi gas model;
- LD model 3. – the generalised super-fluid model;
- LD model 4. – the microscopic level densities based on the Goriely's tables;
- LD model 5. – Hilaire's combinatorial tables;
- LD model 6. – the temperature dependent Hartree-Fock-Bogoliubov model, Gogny force.
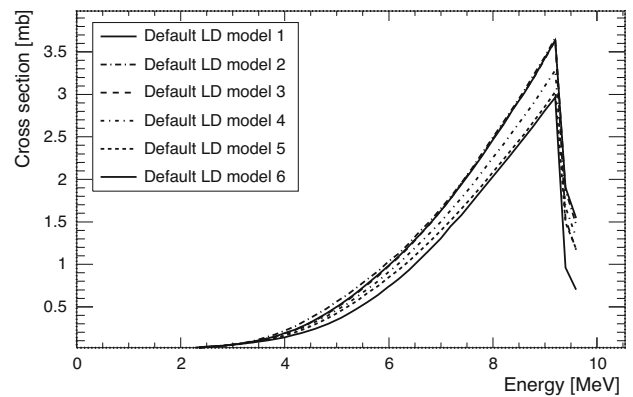


**Fig. 6** Default functions for the $^{115}$In$(\gamma, \gamma')^{115m}$In cross-section obtained by TALYS 1.9 for six different level density models (for details see text)
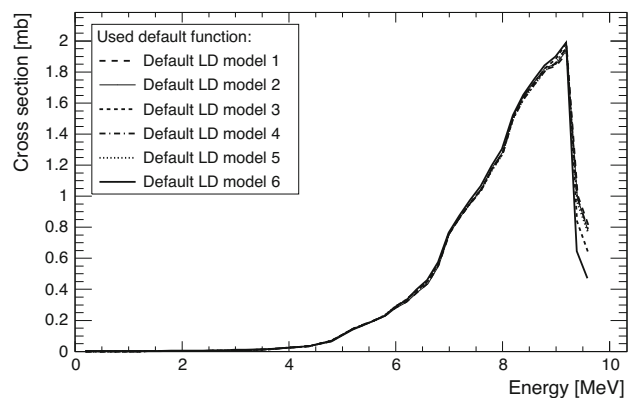


**Fig. 7** Unfolded $^{115}$In$(\gamma, \gamma')^{115m}$In cross-section for each default function, produced using the SANDII unfolding algorithm

Six different excitation functions for the $^{115}$In$(\gamma, \gamma')^{115m}$In reaction were obtained (see Fig. 6) and used as default functions for the unfolding procedures.

Other parameters such as photon strength functions (PSF) can also have a significant impact on cross-section values. However, detailed theoretical analysis was not part of this study and those parameters are not change from the default values given by the TALYS 1.9., which are for example the standard Lorentzian (Brink-Axel model) for PSF.
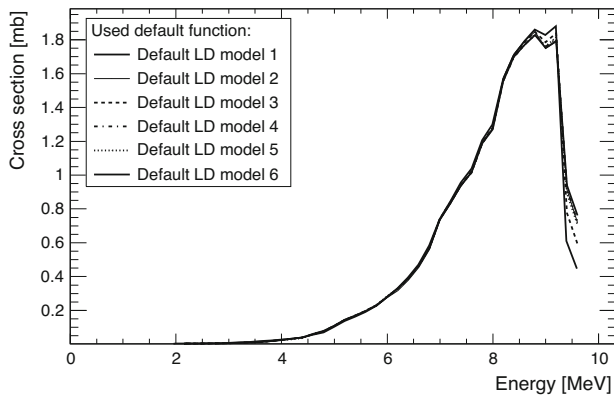
**Fig. 8** Unfolded $^{115}$In$(\gamma, \gamma')^{115m}$In cross-section for each default function, produced using the GRAVEL unfolding algorithm
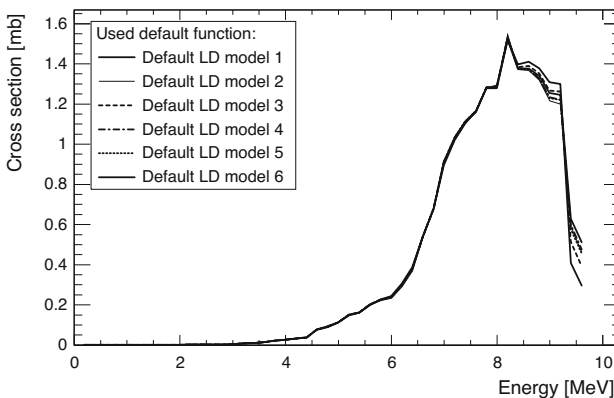


**Fig. 9** Unfolded $^{115}$In$(\gamma, \gamma')^{115m}$In cross-section for each default function, produced using the MAXED unfolding algorithm

### 4.2 Unfolding results

Three unfolding algorithms were used in this work and their results were compared. The first one was the SANDII iterative algorithm [27], the second was the GRAVEL algorithm, which is an improved version of SANDII [26] and, the third one was the MAXED algorithm that uses the maximum entropy principle to calculate the unfolded function [23].

The SANDII and GRAVEL algorithm give the solution:

$$\sigma_i^{J+1} = \sigma_i^J f(A_k \epsilon_k \Phi_{ki} \sigma_i^J)$$

$$f = \exp \left( \frac{\sum_{k=1}^m W_{ik}^J \ln \left( \frac{A_k}{\sum_{i=1}^n W_{ik}^J \sigma_i^J} \right)}{\sum_{k=1}^m W_{ik}^J} \right), i = 1, 2...n$$

$$(4)$$

where in the case of the SANDII $W_{ik}^J$ is:

$$W_{ik}^J = \frac{\Phi_{ki} \sigma_i^J}{\sum_{i=1}^n \Phi_{ki}^J}.$$

$$(5)$$

and in the case of the GRAVEL $W_{ik}^J$ is:

$$W_{ik}^J = \frac{\Phi_{ki} \sigma_i^J}{\sum_{i=1}^n \Phi_{ki}^J} \frac{A_k^2}{\epsilon_k^2}.$$

$$(6)$$

$A_k$ is measured saturated activity, $\epsilon_k$ is measured uncertainty, cross-section for energy bin $E_i$ is $\sigma_i$ and photon flux is $\Phi_{ki}$ when irradiating $k$ disk at energy bin $E_i$, $J$ is number of the iteration step, $m$ is number of activated discs and $n$ is number of energy bins.

The MAXED algorithm provides by the fitting input data (measured induced specific saturated activity $A_k$), a function $\sigma(E)$ that maximizes the relative entropy:

$$S = - \int \left( \sigma(E) \ln \left( \frac{\sigma(E)}{\sigma_{def}(E)} \right) + \sigma_{def}(E) - \sigma(E) \right) dE$$

$$(7)$$

where $\sigma_{def}(E)$ is the default cross section function.

Unfolding procedures were performed in the energy range between 0 and 9.6 MeV grouped into 48 bins. The results obtained by the SANDII, GRAVEL and MAXED algorithms for all used default functions are presented in Figs. 7, 8 and 9.

### 4.3 Analysis of uncertainties

We will analyse here following sources of uncertainties that could have affect the final results: the measurement of saturated gamma activity, determination of normalisation factor, Monte Carlo calculation of photon spectra and unfolding procedures.

#### 4.3.1 Gamma activation measurement

The uncertainty values of saturated gamma activity were determinated by taking into account contribution of uncertainties of all parameters from Eq. 3, and obtained values are presented in Table 3. Those uncertainties are dominated by statistical error of measurement of gamma peak intensity. Uncertainties of gamma activation measurement are affected the final results. However, only the MAXED algorithm gives the possibility to estimate the error of the cross section values depending on the error of the measured activity, while for the other two algorithms such an error analysis is not possible [43]. Cross section uncertainty of the MAXED code due to saturated gamma activity measurement uncertainty is presented in the first column of Table 5 in the case of the LD model 6 used as default function. Similar results were obtained for other 5 default functions. The influence of the measured gamma activity uncertainty on the error of the final results using other algorithms requires additional analyses that are not part of this study.

**Fig. 10** Spectra of photon flux on the indium disks for 10 MeV endpoint energy obtained by different models: EMstandard, EM standard_opt3, EMLivermore and EMPenelope
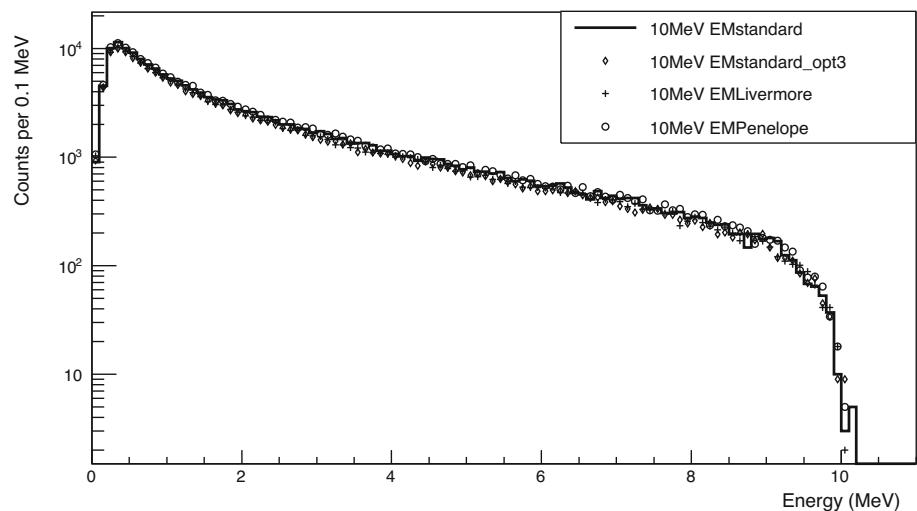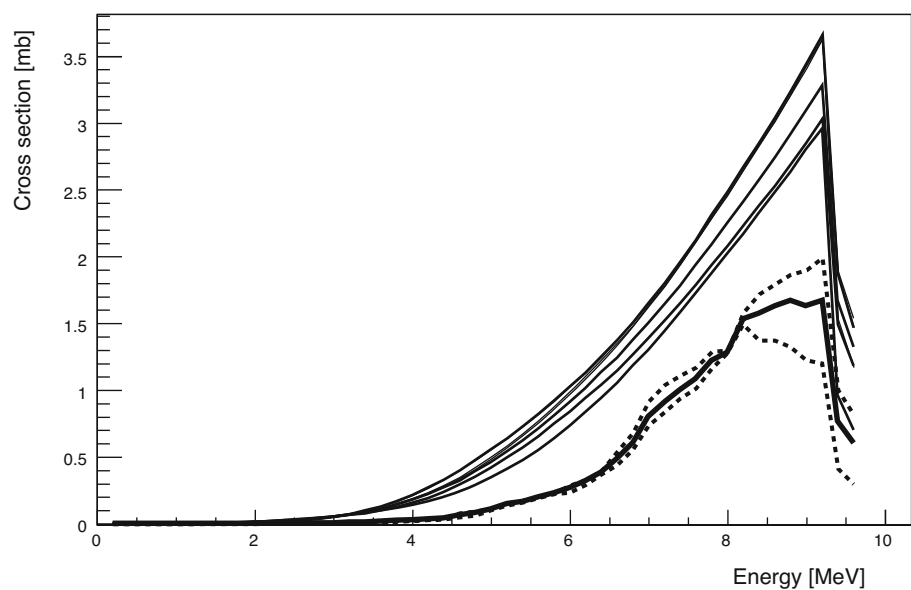


**Fig. 11** Unfolded results for the $^{115}$In$(\gamma, \gamma')^{115m}$In cross-section (line with a corridor of uncertainty) in comparison with default TALYS 1.9 functions (Fig. 6)



### 4.3.2 Normalisation factor

The cross section values for the $^{113}In(\gamma, \gamma')^{113m}In$ reaction taken from Ref. [32] were determined with uncertainty that varied form 50 % at low energy to 10% at higher energy. That lead to uncertainty of 17% for normalisation factor which introduced additional uncertainty of the final results obtained in this study. This problem can be solved by introducing precise measurement of photon flux as a part of this technique or by selecting another reaction (with well-known efficient cross-sections) as the standard for normalization.

### 4.3.3 Monte Carlo calculation of photon spectra

In this study, the QBBC model which is recommended for medical and space physics simulations was used [44,45]. Analysis of possible systematic uncertainty introduced by

the choice of the model in the Geant4 simulation was done by comparing results from other available models.

EM standard option model used in the QBBC physics list, as well as previously studied models [46], EM standard option3, Livermore and Penelope, predict the correct absolute scale and are able to reproduce the shape of the energy spectra at forward emission angles, which make the leading contribution to the total radiated energy. Nevertheless, all models over-estimate the bremsstrahlung emission in the backward hemisphere and predict a harder energy distribution than measured [46], which is not the case here, where all bremsstrahlung emission are in the narrow forward region. Obtained results by comparing different models are presented in the Fig 10. Based on those results we consider that the uncertainty introduced by the choice of the model in the Geant4 simulation is negligible.

**Fig. 12** Comparison of the $^{115}$In$(\gamma, \gamma')^{115m}$In cross-section obtained in this work (line with uncertainty bars) with existing experimental data (white circle – [16], black filled square – [17], black filled circle – [18], black filled triangle [19], white square – [20])
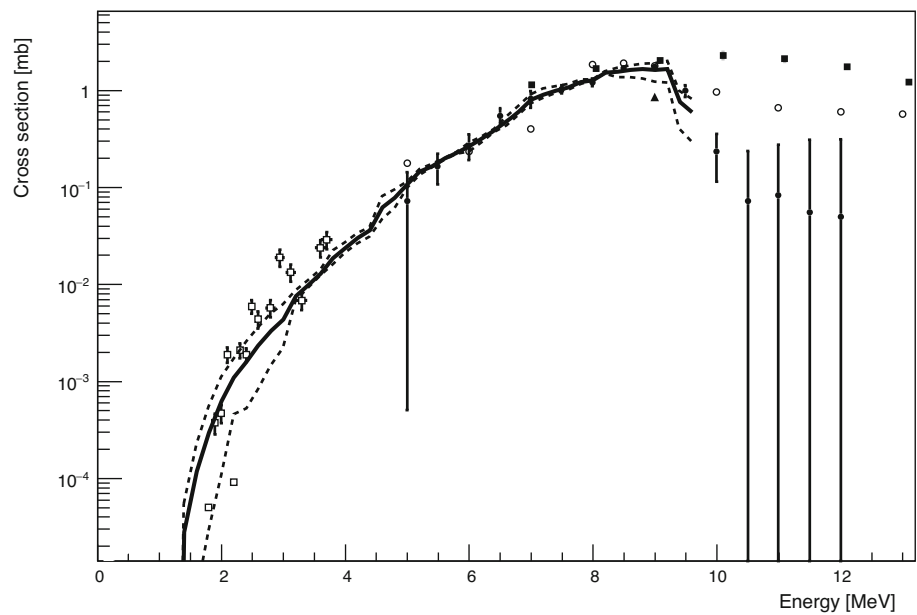


**Table 4** The $\chi^2$ values 8 for: 1. Default functions before unfolding procedures, 2. SANDII results, 3. GRAVEL results and 4. MAXED results

$\chi^2$

| Energy (MeV) | Ld model 1 | Ld model 2 | Ld model 3 | Ld model 4 | Ld model 5 | Ld model 6 |
|---|---|---|---|---|---|---|
| *1. Default functions* | | | | | | |
| 5.00(5) | 253.03 | 280.01 | 252.84 | 272.95 | 282.51 | 297.59 |
| 6.00(5) | 33.40 | 39.41 | 32.73 | 34.67 | 34.81 | 30.09 |
| 7.00(5) | 107.44 | 116.33 | 105.32 | 107.33 | 106.26 | 87.90 |
| 8.20(5) | 0.03 | 0.31 | 0.02 | 0.14 | 0.21 | 0.38 |
| 9.00(5) | 112.89 | 132.55 | 110.05 | 120.70 | 123.58 | 112.17 |
| 10.00(5) | 120.07 | 144.36 | 119.75 | 130.04 | 133.45 | 117.23 |
| *2. SANDII results* | | | | | | |
| 5.00(5) | 0.16 | 0.14 | 0.28 | 0.30 | 0.32 | 0.54 |
| 6.00(5) | 0.58 | 0.51 | 0.62 | 0.64 | 0.66 | 0.90 |
| 7.00(5) | 2.56 | 2.53 | 2.69 | 2.75 | 2.72 | 1.90 |
| 8.20(5) | 0.08 | 0.04 | 0.06 | 0.06 | 0.07 | 0.11 |
| 9.00(5) | 6.55 | 6.72 | 7.27 | 7.77 | 7.62 | 5.62 |
| 10.00(5) | 0.76 | 0.79 | 0.34 | 0.39 | 0.38 | 0.50 |
| *3. GRAVEL results* | | | | | | |
| 5.00(5) | 0.77 | 0.52 | 0.80 | 0.93 | 1.00 | 2.57 |
| 6.00(5) | 0.24 | 0.21 | 0.27 | 0.25 | 0.26 | 0.32 |
| 7.00(5) | 4.80 | 4.46 | 4.45 | 4.70 | 4.61 | 3.59 |
| 8.20(5) | 0.31 | 0.21 | 0.30 | 0.31 | 0.31 | 0.26 |
| 9.00(5) | 4.47 | 4.25 | 4.14 | 4.44 | 4.40 | 3.95 |
| 10.00(5) | 1.01 | 1.15 | 0.91 | 0.97 | 0.96 | 0.79 |
| *4. MAXED results* | | | | | | |
| 5.00(5) | 0.06 | 0.05 | 0.06 | 0.07 | 0.07 | 0.10 |
| 6.00(5) | 0.35 | 0.28 | 0.35 | 0.34 | 0.35 | 0.41 |
| 7.00(5) | 2.73 | 2.62 | 2.72 | 2.64 | 2.60 | 2.76 |
| 8.20(5) | 3.64 | 3.72 | 3.64 | 3.76 | 3.76 | 3.56 |
| 9.00(5) | 3.06 | 2.85 | 2.88 | 2.87 | 2.84 | 2.85 |
| 10.00(5) | 2.16 | 2.50 | 2.33 | 2.32 | 2.40 | 2.33 |

**Table 5** Analysis of uncertainties

| Energy (MeV) | $\sigma_{MAXEDAc}$ (%) | $\sigma_{SANDII}$ (%) | $\sigma_{GRAVEL}$ (%) | $\sigma_{MAXED}$ (%) | $\sigma_U$ (%) | $\sigma_D$ (%) |
|---|---|---|---|---|---|---|
| 0.2 | 8568.00 | 10.94 | 14.21 | 25.59 | 100.49 | 99.99 |
| 0.4 | 3561.00 | 10.79 | 14.45 | 45.28 | 105.83 | 100.00 |
| 0.6 | 341.20 | 10.98 | 14.17 | 35.66 | 105.17 | 100.00 |
| 0.8 | 227.50 | 11.11 | 14.32 | 25.27 | 101.48 | 99.99 |
| 1 | 171.70 | 11.03 | 14.04 | 19.87 | 98.56 | 99.78 |
| 1.2 | 149.10 | 10.96 | 14.32 | 16.56 | 96.92 | 99.56 |
| 1.4 | 123.20 | 11.13 | 14.16 | 13.57 | 95.09 | 98.14 |
| 1.6 | 85.50 | 11.12 | 14.00 | 12.44 | 86.72 | 94.71 |
| 1.8 | 81.27 | 10.98 | 14.15 | 10.82 | 85.21 | 90.20 |
| 2 | 52.99 | 11.10 | 13.98 | 12.17 | 74.33 | 83.02 |
| 2.2 | 55.47 | 10.89 | 13.68 | 8.35 | 56.57 | 58.67 |
| 2.4 | 47.59 | 10.92 | 13.71 | 10.13 | 61.19 | 66.70 |
| 2.6 | 44.83 | 10.51 | 12.97 | 10.26 | 56.38 | 63.56 |
| 2.8 | 31.66 | 9.47 | 12.17 | 10.88 | 48.19 | 57.08 |
| 3 | 36.10 | 7.68 | 10.34 | 8.25 | 40.95 | 49.71 |
| 3.2 | 20.04 | 5.59 | 7.92 | 4.86 | 14.57 | 11.22 |
| 3.4 | 17.51 | 3.23 | 5.60 | 3.03 | 11.16 | 6.88 |
| 3.6 | 13.32 | 1.44 | 3.54 | 1.58 | 8.85 | 5.50 |
| 3.8 | 10.30 | 1.42 | 1.72 | 1.07 | 20.42 | 13.81 |
| 4 | 7.42 | 2.59 | 1.54 | 1.30 | 12.16 | 12.01 |
| 4.2 | 7.73 | 3.68 | 2.26 | 1.60 | 10.48 | 13.41 |
| 4.4 | 8.01 | 4.36 | 2.67 | 2.28 | 8.58 | 13.76 |
| 4.6 | 15.53 | 4.03 | 3.26 | 2.58 | 29.84 | 24.26 |
| 4.8 | 13.53 | 3.86 | 3.20 | 2.08 | 21.77 | 20.88 |
| 5 | 16.38 | 2.84 | 2.88 | 0.85 | 6.23 | 8.65 |
| 5.2 | 12.87 | 2.17 | 2.73 | 0.89 | 4.87 | 8.13 |
| 5.4 | 9.82 | 1.57 | 2.03 | 0.47 | 4.20 | 4.11 |
| 5.6 | 7.14 | 0.89 | 1.47 | 0.38 | 1.26 | 4.09 |
| 5.8 | 9.05 | 0.75 | 0.94 | 0.64 | 1.74 | 2.63 |
| 6 | 11.47 | 1.07 | 0.61 | 1.26 | 7.86 | 12.82 |
| 6.2 | 11.67 | 1.72 | 1.09 | 1.32 | 4.67 | 8.03 |
| 6.4 | 8.48 | 1.61 | 1.03 | 1.38 | 2.64 | 4.03 |
| 6.6 | 6.55 | 1.53 | 0.86 | 0.14 | 11.59 | 9.67 |
| 6.8 | 4.47 | 1.35 | 1.03 | 0.33 | 12.83 | 8.67 |

### 4.3.4 Unfolding procedures

The validation of the unfolding results was done by calculating an induced activity ($A_c = \sum \sigma(E_i) \cdot \Phi(E_i) \cdot \Delta E$) and subsequent comparison with the measured data ($A_k$, Table 3). This was done for all default cross-section functions and for all three algorithms, SANDII, GRAVEL and MAXED. In Table 4, the $\chi^2$ values are presented:

$$\chi^2 = \frac{(A_c - A_k)^2}{\sigma_{A_k}^2} \qquad (8)$$

These results suggested that unfolding results can reproduce the measured values of $A_k$ much more accurately than the default functions.

For all three unfolding algorithms averaged cross sections for all variants of default function were calculated. The standard deviations from average values for algorithms are presented in Table 5. The objective of this study was not to judge which of the three unfolding algorithms would give most realistic results. Therefore, we treated all obtained cross sections with equal weights in the following. The final result, depicted in Fig. 11, represents the cross section averaged over all 18 variants, i.e. three unfolding codes and six default functions.

**Table 5** continued

| Energy (MeV) | $\sigma_{MAXEDAc}$ (%) | $\sigma_{SANDII}$ (%) | $\sigma_{GRAVEL}$ (%) | $\sigma_{MAXED}$ (%) | $\sigma_U$ (%) | $\sigma_D$ (%) |
|---|---|---|---|---|---|---|
| 7 | 7.04 | 0.21 | 0.21 | 0.81 | 14.30 | 8.32 |
| 7.2 | 6.02 | 0.46 | 0.53 | 0.63 | 13.90 | 8.67 |
| 7.4 | 4.55 | 0.64 | 0.62 | 0.34 | 11.14 | 6.61 |
| 7.6 | 3.69 | 0.78 | 0.74 | 0.19 | 8.43 | 5.87 |
| 7.8 | 5.62 | 0.81 | 0.62 | 0.23 | 5.81 | 4.21 |
| 8 | 3.46 | 0.77 | 0.66 | 0.34 | 1.45 | 0.81 |
| 8.2 | 7.03 | 0.67 | 0.53 | 0.61 | 3.01 | 2.64 |
| 8.4 | 5.60 | 0.67 | 0.43 | 0.58 | 9.07 | 12.84 |
| 8.6 | 5.19 | 0.70 | 0.60 | 1.06 | 9.94 | 16.22 |
| 8.8 | 5.06 | 0.62 | 0.59 | 1.48 | 11.44 | 20.89 |
| 9 | 6.35 | 1.05 | 1.51 | 2.39 | 16.41 | 25.35 |
| 9.2 | 5.12 | 1.18 | 1.65 | 2.65 | 18.73 | 28.26 |
| 9.4 | 3.83 | 14.44 | 13.97 | 13.30 | 31.07 | 46.82 |
| 9.6 | 3.79 | 17.09 | 16.59 | 16.29 | 36.01 | 50.74 |

$\sigma_{MAXEDAc}$ cross section uncertainty of MAXED code due to measurement uncertainty, $\sigma_{SANDII}$ standard deviation of average SANDII results, $\sigma_{GRAVEL}$ standard deviation of average GRAVEL results, $\sigma_{MAXED}$ standard deviation of average MAXED results, $\sigma_U$ upper limit of final results, $\sigma_D$ down limit of final results

The solid line represents the averaged cross section. Dashed lines depict the maximum and minimum values of the cross sections representing uncertainty corridor obtained directly from the spectrum unfolding which is also presented in Table 5 ($\sigma_U$ and $\sigma_D$).

It turns out that the LD model 2 of the MAXED code gives the lowest estimation of the cross section. The maximum amplitude of the unfolded cross section is obtained with SANDII code using the LD model 4. In this way the region of the most probable values for the $^{115}$In$(\gamma, \gamma')^{115m}$In reaction cross section, i.e. the uncertainty, was estimated.

In this way, the direct contributions to the uncertainty of the final result from the the measured gamma activity and the normalization factor were not taken into account and that will be part of a future study during the development of this technique.

## 5 Discussion

According to the TALYS 1.9 calculations, the cross section for a selected nuclear reaction channel can be calculated using different nuclear level density models. In Fig. 6 all TALYS 1.9 calculations of the $^{115}$In$(\gamma, \gamma')^{115m}$In differential cross-section have a very similar shape. The only difference may be observed in the amplitude of the functions. It is evident, all TALYS 1.9 calculated cross sections show an exponential growth with increasing energy. When the process of neutron emission starts to compete with the process of de-excitation through electromagnetic transition, the cross section for the $^{115}$In$(\gamma, \gamma')^{115m}$In reaction drops

sharply. According to TALYS 1.9, this happens at around 9 MeV.

Results obtained with three different unfolding algorithms are depicted individually in Figs. 7, 8 and 9. One can see a very interesting trend on them. Differences in the calculated cross sections, presented in Fig. 6, which are not large but still visible, do not produce a significant scatter in the values of the cross section obtained by one single code. For example, different default functions, when used as an input for the SANDII unfolding procedure, give very similar functions describing the cross section (Fig. 7). The same can be seen with the other two codes (Figs. 8, 9). Comparison of the results of three different algorithms, shows that SANDII and GRAVEL give functions of a very similar shape, with a small difference just at maximum energy. Results obtained by the MAXED code predicts slightly different form of the energy differential cross section for the $^{115}$In$(\gamma, \gamma')^{115m}$In reaction. The maximum of the MAXED function is shifted towards 8 MeV, while SANDII predicts that the maximum cross-section value could be at 9 MeV, very similar to the TALYS 1.9 calculations.

Sharp peaks and small discontinuities can be noticed in the results obtained by applying the GRAVEL and the MAXED codes in high energy region above 6 MeV. With a reasonable assumption that the cross section of the $^{115}$In$(\gamma, \gamma')^{115m}$In reaction should be smooth in the region where a giant dipole resonance is dominant mechanism of excitation of nuclei, it may be concluded that these peaks originate from some numerical phenomena related to the algorithm itself. The number and amplitude of these peaks increase in cases, where

the reconstruction of the cross section is performed with a larger number of bins.

It can be seen in Fig. 11 that in the energy interval up to 8 MeV there is a very nice agreement between average, smallest and largest estimation of the cross section, leaving us with a very small systematic uncertainty introduced by the different unfolding algorithms. The differences appear in the region between 8 and 10 MeV. The same figure shows all six results from TALYS 1.9 calculations used as default functions. It can be seen that, without special adjustments, TALYS 1.9 gives significantly higher predictions for the cross-section than that obtained from the unfolding of our data. For this reason, there is a large difference between the saturation activities measured and calculated using the cross section estimated on the basis of the TALYS 1.9 calculations, as shown by $\chi^2$ in Table 4.

The obtained average function was compared with existing experimental data from literature, which are unfortunately not very abundant. Figure 12 depicts the comparison of our results (full line) with data from different authors [16–20], presented by symbols. Most of the data generally shows the same trend, i.e. a growth up to 9 MeV, after which the cross section sharply decrease. In the low-energy region, up to about 4 MeV, our results show the same trend as the data from Ref. [20]. This data is scattered around the line representing our data, obtained by the unfolding technique. The biggest difference between our data and the one from Ref. [20] is around 3 MeV, where our estimation is five times smaller. There is still some room for improvements by using for irradiation photon spectra with endpoint energy less then 5 MeV. It should be noted here that in low-energy region, up to 3 MeV where the excitation of individual levels is possible, some structural effects in the cross section curve should be expected. It is probably a reason of the scatter of the measurements published in reference [20]. Initial TALYS 1.9 function did not take into account the structural effects at low energies.

In the energy region between 5 MeV and 10 MeV the agreement between unfolding results and previous measurements is much better. For example, cross-sections obtained in this project and values published in Ref. [18], presented by closed circles on Fig. 12, are consistent within experimental uncertainties declared by the authors in Ref. [18] and our corridor defined by highest and lowest estimation as presented in Fig. 11. A distinct difference appears at 9 MeV only, where our estimation of the cross-section is 30 % lower. The point at 5 MeV in reference [18] was determined with very large uncertainty. Cross-section values published in reference [17], presented by black squares at Fig. 12 differ from our results up to 35 %. In energy region above 6.5 MeV our values are systematically lower, however, it is interesting to note that in measurements referred in this reference, there is no sharp drop of the cross-section after neutron emission threshold

energy at all. The maximum of cross section function presented in this publication is at 10 MeV and minimum of the cross section peak is in energy region between 15 MeV and 18 MeV. Authors used $^{63}Cu(\gamma,n)^{62}Cu$ and absolute ionisation chamber gor calibration and control of bremsstrahlung beam. Authors used [33] algorithm for calculation. The results published in the reference [16] show maximum of cross section peak at 9 MeV, with the drop at energies higher than the binding energy of neutrons, although not so sharp as presented in reference [18]. Values presented in this reference (◦—in Fig. 12) are scattered around our results with a maximum deviation of 50 %. Authors of publication [16] used NaI detectors for gamma spectra measurements and ionisation chamber with 7.5 cm thick aluminium walls for reconstruction of photon flux spectra. No information related to calculation cross section function were not presented.

To reveal possible factors, which could affect the cross-section values obtained in this study, we can start from the function describing the flux of the bremsstrahlung photons in Eqs. 1 and 2. This function was obtained by simulation with a reasonable number of incident electrons, from the point of view of the duration of a typical GEANT4 simulation. The amplitude of this function was calculated by normalization based on the measured intensity of $^{113m}In$ gamma line of $E_\gamma$ = 391.7 keV in obtained spectra. This was the only way to determine the flux of photons striking the target and, probably, some new method should be developed in a subsequent measurement campaign. Best candidates for new normalisation procedure could be the $(\gamma, \gamma')$ reaction on $^{11}B$ or the $^{115}In(\gamma, n)^{114m}In$ reaction.

## 6 Conclusions

The results presented in this work demonstrates the successful application of the NAXSUN technique also in the field of photonuclear reactions. We suggest that this method has potential in reconstructing energy differential cross sections using activation data from photonuclear reactions. The method was tested in the low-energy region, up to an endpoint energy of 10 MeV, on the example of photoactivation of the $^{115}In$ isomeric state, where it was sufficient to monitor the intensity of only one nicely isolated gamma line in the spectrum. If additional checks confirm the potential of this method, one of the possible applications could be in determining the cross section functions of $(\gamma,xn)$ photonuclear reactions with the emission of more than one neutron, for a number of irradiated nuclei and reaction products (having sufficiently long half-life). For now, only average cross-sections can be found in literature for these nuclear reactions [2,3,47,48], and there are no experimentally established energy differential cross-sections for photonuclear reactions with multiple neutron emission at all.

In this paper, TALYS 1.9 calculations are used to construct the default functions, and the question remains for future work, whether it is possible to expand the method of determining the default function using mean values of efficient cross section as in the case of neutron induced nuclear reactions presented in our previous work [11]. This might be an interesting attempt, although the results of this work shows that the impact of a different choice of a default function obtained by only one selected code on the final result is not crucial.

In our analysis, different results were observed by three different algorithms. Differences are the most significant between the MAXED and the other two of the algorithms (Figs. 7, 8, 9). The obtained results are encouraging enough, but they also open the necessity of subsequent experimental activities in which it will be possible to check, which of the used unfolding codes gives the most reliable approximation to the real cross-section value.

Although the differential cross-section of $^{115}$In$(\gamma, \gamma')^{115m}$In was not of primary interest in this project, it is worth to notice that good agreement with previously published results was obtained. Some of the existing measurement results are quite different, especially at energies higher than 10 MeV [16–18], but it has been observed that they show quite good agreement in the energy range from 5 to 10 MeV. In the same area, our results are fully consistent with literature data.

**Data Availability Statement** This manuscript has no associated data or the data will not be deposited. [Authors' comment: The data can be available on request sent to the corresponding author.]

## References

1. T. Kawano, Y. Cho, P. Dimitriou, D. Filipescu, N. Iwamoto, V. Plujko, X. Tao, H. Utsunomiya, V. Varlamov, R. Xu, R. Capote, I. Gheorghe, O. Gorbachenko, Y. Jin, T. Renstrøm, M. Sin, K. Stopani, Y. Tian, G. Tveten, J. Wang, T. Belgya, R. Firestone, S. Goriely, J. Kopecky, M. Krtička, R. Schwengner, S. Siem, M. Wiedeking, Nucl. Data Sheets **163**, 109 (2020a). https://doi.org/10.1016/j.nds.2019.12.002
2. Experimental nuclear reaction data (exfor). https://www-nds.iaea.org/exfor/exfor.htm. Accessed 22 July 2021
3. N. Otuka, E. Dupont, V. Semkova, B. Pritychenko, A. Blokhin, M. Aikawa, S. Babykina, M. Bossant, G. Chen, S. Dunaeva, R. Forrest, T. Fukahori, N. Furutachi, S. Ganesan, Z. Ge, O. Gritzay, M. Herman, S. Hlavač, K. Katō, B. Lalremruata, Y. Lee, A. Makinaga, K. Matsumoto, M. Mikhaylyukova, G. Pikulina, V. Pronyaev, A. Saxena, O. Schwerer, S. Simakov, N. Soppera, R. Suzuki, S. Takács, X. Tao, S. Taova, F. Tárkányi, V. Varlamov, J. Wang, S. Yang, V. Zerkin, Y. Zhuang, Nucl. Data Sheets **120**, 272 (2014)
4. The ENDF, evaluated nuclear data file. https://www-nds.iaea.org/exfor/endf.htm. Accessed 22 July 2021
5. D. Brown, M. Chadwick, R. Capote, A. Kahler, A. Trkov, M. Herman, A. Sonzogni, Y. Danon, A. Carlson, M. Dunn, D. Smith, G. Hale, G. Arbanas, R. Arcilla, C. Bates, B. Beck, B. Becker, F. Brown, R. Casperson, J. Conlin, D. Cullen, M.-A. Descalle, R. Firestone, T. Gaines, K. Guber, A. Hawari, J. Holmes, T. John-

son, T. Kawano, B. Kiedrowski, A. Koning, S. Kopecky, L. Leal, J. Lestone, C. Lubitz, J.M. Damián, C. Mattoon, E. McCutchan, S. Mughabghab, P. Navratil, D. Neudecker, G. Nobre, G. Noguere, M. Paris, M. Pigni, A. Plompen, B. Pritychenko, V. Pronyaev, D. Roubtsov, D. Rochman, P. Romano, P. Schillebeeckx, S. Simakov, M. Sin, I. Sirakov, B. Sleaford, V. Sobes, E. Soukhovitskii, I. Stetcu, P. Talou, I. Thompson, S.V.D. Marck, L. Welser-Sherrill, D. Wiarda, M. White, J. Wormald, R. Wright, M. Zerkle, G. Žerovnik, Y. Zhu, Nucl. Data Sheets **148**, 1 (2018)
6. IAEA photonuclear data. https://www-nds.iaea.org/photonuclear/pdfilelist.html. Accessed 22 July 2021
7. T. Kawano, Y. Cho, P. Dimitriou, D. Filipescu, N. Iwamoto, V. Plujko, X. Tao, H. Utsunomiya, V. Varlamov, R. Xu, R. Capote, I. Gheorghe, O. Gorbachenko, Y. Jin, T. Renstrøm, M. Sin, K. Stopani, Y. Tian, G. Tveten, J. Wang, T. Belgya, R. Firestone, S. Goriely, J. Kopecky, M. Krtička, R. Schwengner, S. Siem, M. Wiedeking, Nucl. Data Sheets **163**, 109 (2020b). https://doi.org/10.1016/j.nds.2019.12.002
8. Janis nuclear data. https://www.oecd-nea.org/jcms/pl_39910/janis. Accessed 22 July 2021
9. G. Lövestam, M. Hult, A. Fessler, T. Gamboni, J. Gasparro, W. Geerts, R. Jaime, P. Lindahl, S. Oberstedt, H. Tagziria, Nucl. Instrum. Methods Phys. Res. Sect. A Accel. Spectrom. Detect. Assoc. Equip. **580**, 1400 (2007)
10. L. Daraban, N. Jovančević, S. Oberstedt, F.-J. Hambsch, Phys. Procedia **59**, 138 (2014)
11. N. Jovancevic, L. Daraban, S. Oberstedt, Nuclear Instrum. Methods Phys. Res. Sect. A Accel. Spectrom. Detect. Assoc. Equip. **739**, 68 (2014)
12. N. Jovančević, L. Daraban, H. Stroh, S. Oberstedt, M. Hult, C. Bonaldi, W. Geerts, F.-J. Hambsch, G. Lutter, G. Marissens et al., Eur. Phys. J. A **52**, 148 (2016)
13. S. Ilić, N. Jovančević, L. Daraban, H. Stroh, S. Oberstedt, M. Hult, C. Bonaldi, W. Geerts, F.-J. Hambsch, G. Lutter, G. Marissens, M. Vidali, D. Knežević, Eur. Phys. J. A **56**, 202 (2020)
14. E. Browne, R. Firestone, *Table of Radioactive Isotopes* (Wiley, New York, 1986)
15. J. Kopecky, J. Sublet, J. Simpson, R. Forrest, D. Nierop, Atlas of neutron capture cross sections (International Atomic Energy Agency (IAEA). INDC(NDS)-362 (1997)
16. O. Bogdankevich, L. Lazareva, F. Nikolaev, J. Exp. Theor. Phys. **4**, 320 (1957)
17. V. Bokhinyuk, A.I. Guthy, A.M. Parlag, M.T. Sabolchy, I.V. Sokolyuk, I.V. Khimich, Ukr. J. Phys. **51**, 657 (2006)
18. V. Mazur, I. Sokolyuk, Z. Bigan, I. Kobal, Phys. At. Nuclei **56**, 10 (1993)
19. N. Demekhina, A. Danagulyan, G. Karapetyan, Phys. At. Nuclei **64**, 1796 (2001)
20. W. Tornow, M. Bhike, S. Finch, A. Krishichayan, Phys. Rev. C **98**, 064305 (2018)
21. Talys nuclear code. https://tendl.web.psi.ch/tendl_2019/talys.html. Accessed 22 July 2021
22. A. Koning, D. Rochman, Nucl. Data Sheets **113**, 2841 (2012). https://doi.org/10.1016/j.nds.2012.11.002. (**special Issue on Nuclear Reaction Data**)
23. M. Reginatto, P. Goldhagen, Health Phys. **77**, 579 (1999)
24. W.L. Goffe, Stud. Nonlinear Dyn. Econom. **1**(3), (1996). https://doi.org/10.2202/1558-3708.1020
25. R. Behrens, J. Instrum. **4**, P03027 (2009)
26. M. Matzke, Report PTB-N-19 I–IV (1994)
27. W.N. McElroy, S. Berg, T. Crockett, Los Alamos National Laboratory report, AFWL-TR-67-41 I–IV (1967)
28. 25-microtron. http://flerovlab.jinr.ru/mt-25-microtron/. Accessed 22 July 2021

29. M. Krmar, Y. Teterev, A. Belov, S. Mitrofanov, Nucl. Instrum. Methods Phys. Res. Sect. A Accel. Spectrom. Detect. Assoc. Equip. **901**, 133 (2018). https://doi.org/10.1016/j.nima.2018.06.028

30. B. Forkman, R. Petersson, *Photonuclear cross-sections in Handbook on Nuclear Activation data* (Technical Reports Series No. 273, IAEA, Vienna, 1987)

31. S. Agostinelli, J. Allison, K. Amako, J. Apostolakis, H. Araujo, P. Arce, M. Asai, D. Axen, S. Banerjee, G. Barrand, F. Behner, L. Bellagamba, J. Boudreau, L. Broglia, A. Brunengo, H. Burkhardt, S. Chauvie, J. Chuma, R. Chytracek, G. Cooperman, G. Cosmo, P. Degtyarenko, A. Dell'Acqua, G. Depaola, D. Dietrich, R. Enami, A. Feliciello, C. Ferguson, H. Fesefeldt, G. Folger, F. Foppiano, A. Forti, S. Garelli, S. Giani, R. Giannitrapani, D. Gibin, J. Gómez Cadenas, I. González, G. Gracia Abril, G. Greeniaus, W. Greiner, V. Grichine, A. Grossheim, S. Guatelli, P. Gumplinger, R. Hamatsu, K. Hashimoto, H. Hasui, A. Heikkinen, A. Howard, V. Ivanchenko, A. Johnson, F. Jones, J. Kallenbach, N. Kanaya, M. Kawabata, Y. Kawabata, M. Kawaguti, S. Kelner, P. Kent, A. Kimura, T. Kodama, R. Kokoulin, M. Kossov, H. Kurashige, E. Lamanna, T. Lampén, V. Lara, V. Lefebure, F. Lei, M. Liendl, W. Lockman, F. Longo, S. Magni, M. Maire, E. Medernach, K. Minamimoto, P. Mora de Freitas, Y. Morita, K. Murakami, M. Nagamatu, R. Nartallo, P. Nieminen, T. Nishimura, K. Ohtsubo, M. Okamura, S. O'Neale, Y. Oohata, K. Paech, J. Perl, A. Pfeiffer, M. Pia, F. Ranjard, A. Rybin, S. Sadilov, E. Di Salvo, G. Santin, T. Sasaki, N. Savvas, Y. Sawada, S. Scherer, S. Sei, V. Sirotenko, D. Smith, N. Starkov, H. Stoecker, J. Sulkimo, M. Takahata, S. Tanaka, E. Tcherniaev, E. Safai Tehrani, M. Tropeano, P. Truscott, H. Uno, L. Urban, P. Urban, M. Verderi, A. Walkden, W. Wander, H. Weber, J. Wellisch, T. Wenaus, D. Williams, D. Wright, T. Yamada, H. Yoshida, D. Zschiesche, Nucl. Instrum. Methods Phys. Res. Sect. A Accel. Spectrom. Detect. Assoc. Equip. **506**, 250 (2003). https://doi.org/10.1016/S0168-9002(03)01368-8

32. Z. Bigan, V. Zheltonozhsky, V. Kirishchuk, A.D.S.V.M. Mazur, P. Trifonov, Bull. Russ. Acad. Sci. Phys. **70**, 292 (2006)

33. A. Penfold, J. Leiss, Phys. Rev. **114**, 1332 (1959)

34. A. Koning, J. Delaroche, Nucl. Phys. A **713**, 231 (2003)

35. W. Hauser, H. Feshbach, Phys. Rev. **87**, 366 (1952)

36. C. Kalbach, Phys. Rev. C **33**, 818 (1986)

37. A. Gilbert, A. Cameron, Can. J. Phys. **43**, 1446 (1965)

38. W. Dilg, Nucl. Phys. A **217**, 269 (1973)

39. A. Zubov, G. Adamian, N. Antonenko, Phys. Particles Nuclei **40**, 847 (2009)

40. A. Ignatyuk, J. Weil, S. Raman, S. Kahane, Phys. Rev. C **47**, 1504 (1993)

41. S. Goriely, S. Hilaire, A.J. Koning, Phys. Rev. C **78**, 064307 (2008)

42. S. Hilaire, M. Girod, S. Goriely, A.J. Koning, Phys. Rev. C **86**, 064317 (2012)

43. M. Reginatto, P. Goldhagen, S. Neumann, Nucl. Instrum. Methods Phys. Res. Sect. B Beam Interact. Mater. Atoms **476**, 242–246 (2002)

44. A.V. Ivantchenko, V.N. Ivanchenko, J.-M.Q. Molina, S.L. Incerti, Int. J. Radiat. Biol. **88**(1–2), 171–175 (2011). https://doi.org/10.3109/09553002.2011.610865

45. Geant4-userdoc. https://geant4-userdoc.web.cern.ch/UsersGuides/PhysicsListGuide/BackupVersions/V10.6c/html/reference_PL/QBBC.html. Accessed 22 July 2021

46. L. Pandola, C. Andenna, B. Caccia, Nucl. Instrum. Methods Phys. Res. Sect. B Beam Interact. Mater. Atoms **350**, 41 (2015)

47. H. Naik, G. Kim, K. Kim, M. Zaman, A. Goswami, M.W. Lee, S.-C. Yang, Y.-O. Lee, S.-G. Shin, M.-H. Cho, Nucl. Phys. A **948**, 28 (2016). https://doi.org/10.1016/j.nuclphysa.2016.01.015

48. M. Zaman, G. Kim, H. Naik, K. Kim, Y.-S. Cho, Y.-O. Lee, S.-G. Shin, M.-H. Cho, Y.-R. Kang, M.-W. Lee, Nucl. Phys. A **960**, 22 (2017). https://doi.org/10.1016/j.nuclphysa.2017.01.008

**Фотокопија диплома са основних и мастер студија**

РЕПУБЛИКА СРБИЈА

## УНИВЕРЗИТЕТ У НОВОМ САДУ
## ПРИРОДНО-МАТЕМАТИЧКИ ФАКУЛТЕТ, НОВИ САД

Оснивач: Република Србија
Аутономна Покрајина Војводина

Дозволу за рад 106-022-00644/2009-01 од 23.12.2009. године је издала
Аутономна Покрајина Војводина, Покрајински секретаријат за образовање.
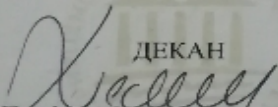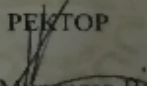
# ДИПЛОМА

## Жарко (Светозар) Медић

рођен 03.02.1988. године у месту Нови Сад, општина Нови Сад, Република Србија, уписан школске 2007/08 године, а дана 19.04.2013. године завршио је Основне академске студије првог степена на студијском програму ФИЗИКА обима 246 (две стотине четрдесет шест) бодова ЕСПБ са просечном оценом 8,84 (осам и 84/100). На основу тога издаје се ова диплома о стеченом високом образовању и стручном називу:

## ДИПЛОМИРАНИ ФИЗИЧАР

Број дипломе: 1262-408/07, 30.10.2013. године
У Новом Саду

ДЕКАН
Проф. др Неда Мимица-Дукић

РЕКТОР
Проф. др Мирослав Весковић

## РЕПУБЛИКА СРБИЈА

# УНИВЕРЗИТЕТ У НОВОМ САДУ
# ПРИРОДНО-МАТЕМАТИЧКИ ФАКУЛТЕТ, НОВИ САД

Оснивач: Република Србија
Аутономна Покрајина Војводина
Дозволу за рад 114-022-423/2012-01 од 18. 09. 2012. године је издала
Аутономна Покрајина Војводина, Покрајински секретаријат за науку и технолошки развој

# ДИПЛОМА

## Жарко (Светозар) Медић

рођен 03. 02. 1988. године у Новом Саду, општина Нови Сад, Република Србија, уписан школске 2013/2014. године, а дана 05. 12. 2014. године завршио је мастер академске студије другог степена на студијском програму ФИЗИКА обима 60 (шездесет) бодова ЕСПБ са просечном оценом 10,00 (десет и 00/100).

На основу тога издаје се ова диплома о стеченом високом образовању и академском називу

## МАСТЕР ФИЗИЧАР

Број дипломе: 1939-М-256m/13, 08. 02. 2016. године
У Новом Саду

ДЕКАН
Проф. др Милица Павков Хрвојевић

РЕКТОР
Проф. др Душан Николић

UNS08MA03845

# Потврда о прихватању теме докторске тезе

Број: 0603-286/21 — 11
Датум: 11. 10. 2021

ПРОФ. ДР МИОДРАГ КРМАР
Департман за физику

Предмет: обавештење **менторима** о прихваћеној
оцени подобности теме
докторске дисертације.

Обавештавамо Вас да је Наставно-научно веће Природно-математичког факултета у Новом Саду на **36** седници одржаној **16.09.2021.** године, прихватило тему докторске дисертације под насловом: „Одређивање ефикасног пресека реакције $^{115}In(\gamma,\gamma')^{115m}In$ у енергетском опсегу од 0 до 9,6 MeV" „Determining cross section of the reaction $^{115}In(\gamma,\gamma')^{115m}In$ in the energy range from 0 to 9.6 MeV" кандидата Жарка Меиџа.

Сенат Универзитета у Новом Саду на **36** седници одржаној **30.09.2021. године** дало је сагласност на предложену тему.

Сходно Статуту Факултета кандидат је дужан приступити изради докторске дисертације и исту одбранити до **30.09.2021. године**.

С поштовањем,

Самостални стручнотехнички сарадник за студије
и студентска питања – руководилац службе

Тамара Зорић, дипл.правник

Број: 04-29/36
Датум: 30. септембар 2021. године

На основу члана 65 став 6 Закона о високом образовању („Службени гласник РС" број 88/2017, 27/2018 – др. закон, 73/2018, 67/2019, 6/2020 – др. закони, 11/2021 - аутентично тумачење, 67/2021 и 67/2021 - др. закон) и члана 67 и 70 Статута Универзитета у Новом Саду број 01-226/1 од 29. септембра 2020. године, Сенат Универзитета у Новом Саду на 36. седници одржаној 30. септембра 2021. године, једногласно доноси

## О Д Л У К У

Сенат Универзитета даје сагласност на Извештај о подобности теме, кандидата и ментора за израду докторске дисертације са темом *Одређивање ефикасног пресека реакције $^{115}In(\gamma,\gamma')^{115m}In$ у енергетском опсегу од 0 до 9,6 MeV / Determining cross section of the reaction $^{115}In(\gamma,\gamma')^{115m}In$ in the energy range from 0 to 9.6 MeV*, кандидатом Жарком Медићем и ментором др Миодрагом Крмаром, редовним професором Природно-математичког факултета Универзитета у Новом Саду.

Кандидату Жарку Медићу одобрава се израда докторске дисертације *Одређивање ефикасног пресека реакције $^{115}In(\gamma,\gamma')^{115m}In$ у енергетском опсегу од 0 до 9,6 MeV / Determining cross section of the reaction $^{115}In(\gamma,\gamma')^{115m}In$ in the energy range from 0 to 9.6 MeV*, на Природно-математичком факултету Универзитета у Новом Саду.

## О б р а з л о ж е њ е

Наставно-научно веће Природно-математичког факултета Универзитета у Новом Саду на седници одржаној 16. септембра 2021. године усвојило је Извештај о подобности теме, кандидата и ментора за израду докторске дисертације са темом *Одређивање ефикасног пресека реакције $^{115}In(\gamma,\gamma')^{115m}In$ у енергетском опсегу од 0 до 9,6 MeV / Determining cross section of the reaction $^{115}In(\gamma,\gamma')^{115m}In$ in the energy range from 0 to 9.6 MeV*, кандидатом Жарком Медићем и ментором др Миодрагом Крмаром, редовним професором Природно-математичког факултета Универзитета у Новом Саду.

Стручно веће за природно-математичке науке Сената Универзитета у Новом Саду на седници одржаној електронским путем са роком за изјашњавање до 24. септембра 2021. године дало је позитивно мишљење о испуњености услова за давање сагласности на наведени извештај.

На основу одлуке Наставно-научног већа Природно-математичког факултета Универзитета у Новом Саду и позитивног мишљења Стручног већа за природно-математичке науке Сената Универзитета у Новом Саду, донета је одлука као у диспозитиву.

Проф. др Дејан Јакшић
Председник Сената Универзитета